Double electron emission from surfaces via low-energy positrons

I. S. Brandt,* Z. Wei,† J. Kirschner, and F. O. Schumann‡
Max Planck Institut für Mikrostrukturphysik, Weinberg 2, 06120 Halle, Germany

(Received 29 May 2018; revised manuscript received 5 May 2019; published 19 August 2019)

We have studied the electron pair emission process from surfaces due to the impact of a primary low-energy positron. The existence of this process implies a two-step scattering event. We find that the electron pair intensity is on the same scale as the positron-electron pair intensity. This suggests that a significant contribution of the pair intensity is actually due to the emission of three particles, of which two are detected. We also observe a strong material dependence of the coincidence intensity. Similarly to our previous studies with primary electron excitation or photon absorption, NiO is the material that displays the highest coincidence rates. We also note that the electron pair intensity scales with the single electron rate. This was also observed in electron pair emission with primary photons or electrons. This suggests that the coincidence intensity may provide a measure of the electron correlation strength.

DOI: 10.1103/PhysRevB.100.075139

I. INTRODUCTION

The radiation of matter via photons or particles can lead to the emission of electron pairs. This is a well-established fact as evidenced by a large amount of experimental work [1,2]. Whatever the details of the process leading to electron emission are, the electron-electron interaction is a key ingredient. In the case of the absorption of a single photon, this can only lead to the emission of electron pairs if there is a finite electron-electron interaction [3,4]. This double photoemission process (DPE) was further theoretically investigated within a model system in which the interaction strength U was varied. It was found that the intensity scaled with the interaction strength [5]. This stimulated experimental work. The results of primary electron excited pair emission [referred to as the $(e, 2e)$ process] and DPE measurements on a variety of thin films and surfaces demonstrated a clear material dependence [6–8]. They also demonstrated an almost monotonic relation between the singles and the coincidence rate. This suggested that the intensity level can serve as a measure of the correlation strength. In a subsequent investigation, we studied the positron-electron pair emission upon positron impact, which we termed (p, ep) [9,10]. In addition to the energy relations of the positron-electron pair, we also discovered a similar material-dependent coincidence intensity.

In this work, we want to explore the electron pair emission due to primary positron impact, which we call $(p, 2e)$ in the following. A single binary collision of a primary electron/positron can lead to the emission of an electron or positron-electron pair. For a finite $(p, 2e)$ intensity, one requires two subsequent collision events. In this case, it is not obvious whether the aforementioned material dependence is preserved. Interestingly, we observe a similar material dependence. Also, the relation between the singles and the coincidence rate is preserved.

This is a surprising result given the very different microscopic effects leading to pair emission in the various coincidence techniques. This lends more support to the suggestion that the coincidence intensity is intimately related to the electron correlation strength.

The sum energy spectrum reveals a significant contribution in which two electrons are emitted from the valence band without any further energy loss. We will bring this observation into the context of secondary electron emission from surfaces.

II. EXPERIMENT

We utilized an ultrahigh-vacuum (UHV) chamber, which allowed the characterization via Auger spectroscopy and low-energy electron diffraction. For the deposition of metal and oxide films, a number of electron beam evaporators were used. The coincidence spectrometer, sketched in Fig. 1, has been explained in more detail elsewhere [11,12].

The key components are a pair of hemispherical analyzers with a 200 mm mean radius that we call "left" and "right," respectively. Depending on the polarity of the electron-optical potentials, detection of either electrons or positrons can be selected. Channel plates with resistive anodes allow us to record the impact position.

We have developed a positron beam facility on the basis of the radioactive decay of the ^{22}Na isotope as presented in more detail elsewhere [10].

The primary flux on the sample is 3×10^4 positrons per second. The primary positron beam lies within the scattering plane as defined by the lens axes of the two spectrometers. The acceptance angle of the spectrometer lenses is $\pm 15^\circ$ within the scattering plane. For all experiments, the analyzers were set to

*Programa de Pós-Graduação em Ciência e Engenharia de Materiais, Universidade Federal de Santa Catarina, Florianópolis, 88040-900, Brazil.
†College of Materials Science and Engineering, Chongqing University, 400044 Chongqing, People's Republic of China.
‡schumann@mpi-halle.de

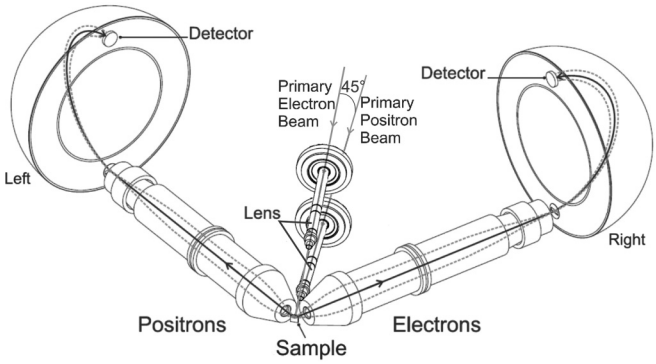

FIG. 1. Two hemispherical analyzers are symmetrically aligned with respect to the surface normal. For (p, ep) measurements, one spectrometer is tuned to positron detection by reversing the polarity applied to the relevant components. For $(e, 2e)$ and $(p, 2e)$ studies, both spectrometers have identical polarities. A primary positron beam propagates along the surface normal. A primary electron beam for $(e, 2e)$ experiments has an angle of 45° with respect to the scattering plane.

a pass energy of 300 eV. This results in a 27-eV-wide energy window that can be covered in parallel by each spectrometer.

For each valid coincidence event, the arrival time (t_{left} and t_{right}) at the respective detector with respect to the coincidence trigger is known. This allows us to compute the arrival time histogram $dt = t_{\text{left}} - t_{\text{right}}$. The emergence of a peak is evidence of "true" coincidences. This means a pair is emitted due to the impact of a single particle.

Two primary particles can also lead to detectable ("random") coincidences. These unwanted events scale quadratically with the flux. Following standard procedures documented in the literature, we are able to remove the aggregate effect of the "random" coincidences [12–14]. Hence we are able to determine the "true" coincidence rate and energy spectra.

The substrate was a single crystal Ag(100) surface that was cleaned via Ar^+ sputtering and annealing. The preparation of NiO films was done via Ni evaporation in an O_2 atmosphere of 10^{-7} mbar following well-documented recipes [15–20]. All experiments were carried out at room temperature.

The low positron flux forced us to operate the spectrometer with the largest entrance slit of 9 mm. In Fig. 2 we plot the elastic peak for a primary electron and positron beam. While the primary electron peak has a full width at half-maximum (FWHM) of 3.1 eV, the positron beam has a value of 5.1 eV. Both values are smaller than expected for a fully illuminated entrance slit which is 6.75 eV. Obviously for both excitations the effective slit size is smaller. The primary electron beam has a spot size of 1 mm, while the positron beam is significantly larger with 5 mm. Therefore, the effective slit size for the positron beam is larger. Another factor is the different energy spread of the two beams. The electron gun is equipped with a BaO cathode, and we have determined a FWHM of 0.3 eV. A common technique to establish a low-energy positron beam is to use a moderator [21]. Suitable materials, e.g., W, reemit low-energy positrons upon exposure of high-energy positrons from a radioactive source. The resulting spread is about 1 eV.

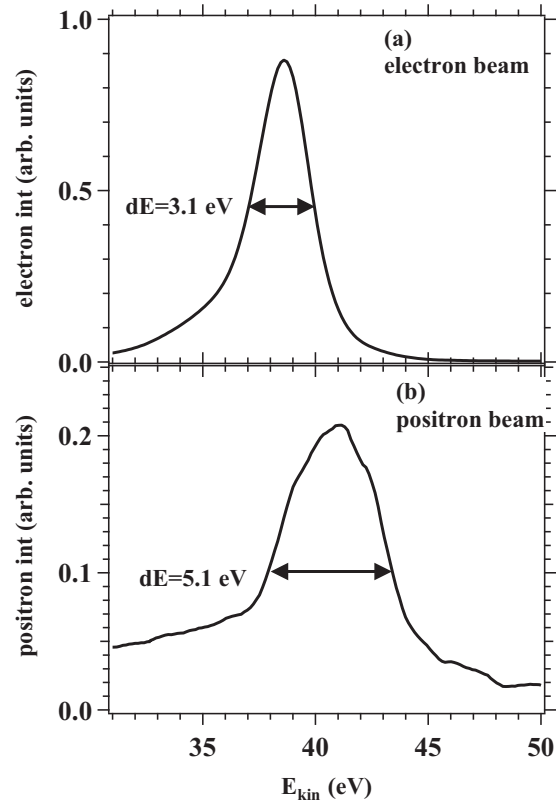

FIG. 2. Elastic peaks for the primary electron (a) and the primary positron beam (b) with energies 38.5 and 41 eV, respectively. These spectra were obtained with the largest entrance slits (9 mm) of the spectrometer and 300 eV pass energy.

This makes an additional contribution of the broadening. More importantly, the positron peak does not show a high-energy cutoff as the electron source, because positrons that are not fully thermalized will be emitted, too.

III. KINEMATICS

We discuss the energy relations for scattering processes relevant for our work and visualize those via energy level diagrams; see Fig. 3. In an $(e, 2e)$ process, a primary electron with kinetic energy E_p^- hits a surface and ejects a valence electron with binding energy E_{vb}^-. We adopt the notation that this energy is measured with respect to the Fermi level E_F and is a positive entity. The emitted electron pair is characterized by the kinetic energies E_1^- and E_2^-, respectively. The superscripts indicate the polarity of the involved primary and emitted particles, which in the case of an $(e, 2e)$ experiment are all negative. We refer these energies to the vacuum level of the sample, which is characterized by the electron work function ϕ. For the energy balance, we can write

$$E_p^- + E_{\text{vb}}^- = E_1^- + E_2^- + \phi = E_{\text{sum}}^{e2e} + \phi. \tag{1}$$

The energy sum of the emitted pair attains the largest value $E_p^- - \phi$ if the valence electron stems from E_F. In analogy to the $(e, 2e)$ process, we write for the energy balance of the (p, ep) process

$$E_p^+ + E_{\text{vb}}^- = E_1^- + E_2^+ + \phi = E_{\text{sum}}^{pep} + \phi. \tag{2}$$

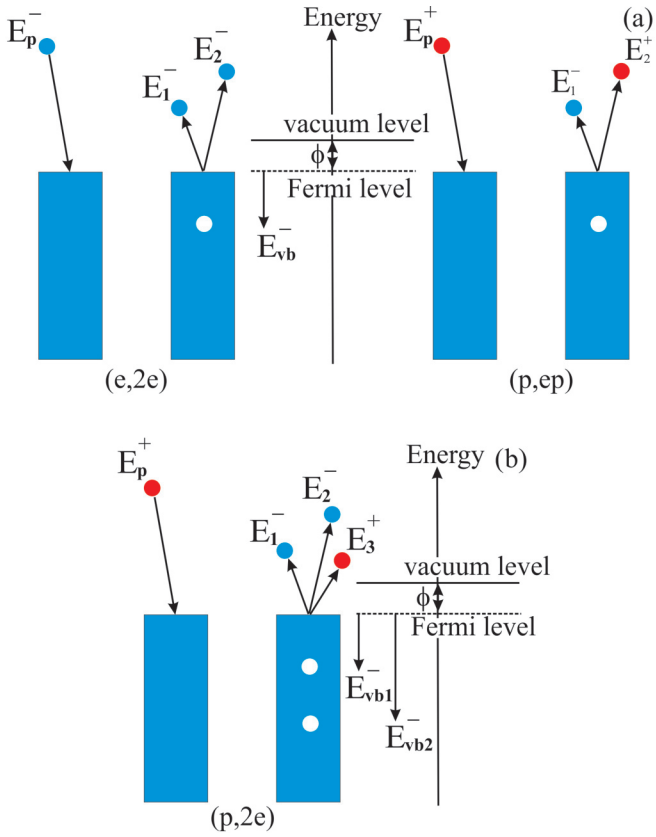

FIG. 3. Energy level diagrams for the $(e, 2e)$, (p, ep), and $(p, 2e)$ processes. The binding energy E_{vb} of the emitted electrons is measured from the Fermi level. We use the convention of positive values. The electron work function is labeled with ϕ. For $(e, 2e)$ and (p, ep) a vacancy in the valence band is created. For $(p, 2e)$ two vacancies in the valence band exist.

Again, the energy sum of the emitted pair has an upper bound that is $E_p^+ - \phi$.

In Fig. 4(a), we sketch a sequence of two binary collisions that leads to triple particle emission. A primary positron interacts with a valence electron. This valence electron escapes the surface while the scattered positron collides with a second valence electron. This is followed by the emission of these two particles. In total, two electrons and the positron leave the sample. We want to term this process as $(p, 2e\,p)$. Another pathway is possible if the positron leaves the sample in the first scattering event while the excited electron interacts with a second electron; see Fig. 4(b). It is straightforward to extend energy conservation to a $(p, 2e\,p)$ process, in which two electrons, with binding energy E_{vb1}^- and E_{vb2}^-, and a positron are emitted:

$$E_p^+ + E_{vb1}^- + E_{vb2}^- = E_1^- + E_2^- + E_3^+ + 2\phi = E_{sum}^{p2ep} + 2\phi. \tag{3}$$

In contrast to the $(e, 2e)$ and (p, ep) processes, one has to consider the work function twice. This means that the maximum energy of the emitted triple is given by $E_p^+ - 2\phi$. This quantity is well-defined for a triple coincidence setup, but our setup does not possess this capability. Therefore, the energy E_3^+ is not known. Hence, we do not expect a sharp

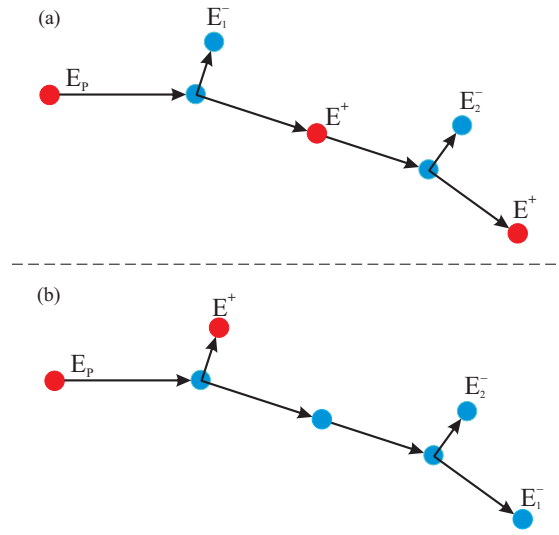

FIG. 4. Schematic view of the two-step scattering mechanism leading to the emission of an electron pair and a positron labeled as the $(p, 2e\,p)$ process. In (a) the positron sequentially scatters with two electrons before leaving the sample. In (b) the positron excites an electron, which in a second step collides with another electron and all three particles leave the sample.

cutoff but a broadened region determined by the range of values adopted by E_3^+. The lowest-energy state of a positron in metal is close to the vacuum level. If we set $E_3^+ = 0$, then we get $E_{sum}^{max} = E_p^+ - 2\phi$, which we want to use as a reference for $(p, 2e)$ experiments.

IV. RESULTS

In Fig. 5, we present the 2D-energy distribution of electron pairs emitted from a NiO surface excited with a 42 eV primary positron beam. The solid diagonal line marks the position of

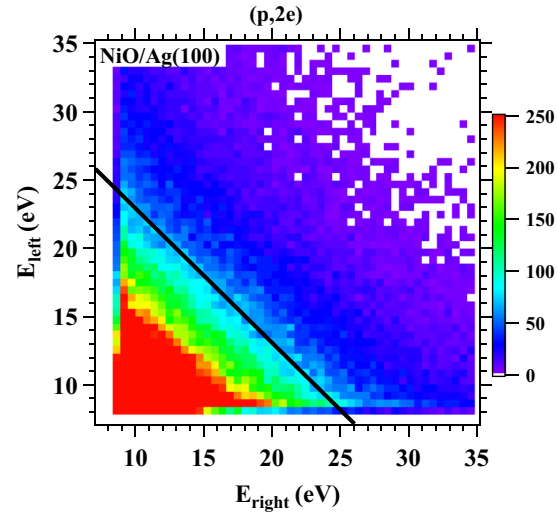

FIG. 5. 2D-energy distributions for $(p, 2e)$ from a 15-ML NiO/Ag(100) film. The primary positron energy was 42 eV. The solid diagonal line marks the value of E_{sum}^{max}.

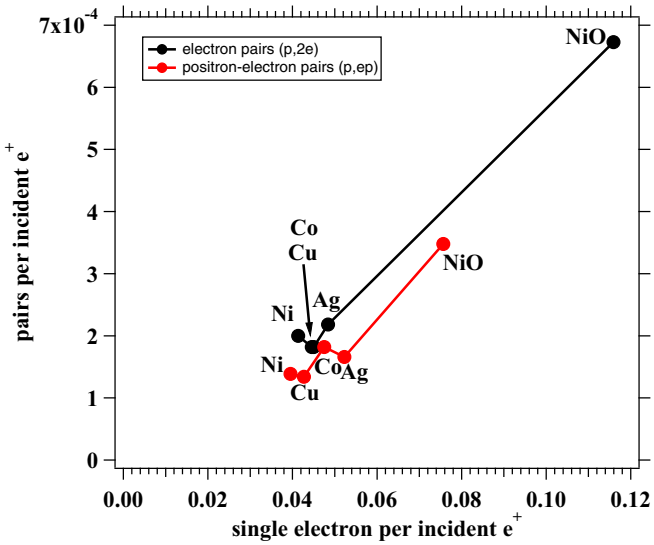

FIG. 6. We display in black the $(p, 2e)$ coincidence intensity per incoming primary positron as a function of the single electron intensity. In red we show the result for the (p, ep) intensity.

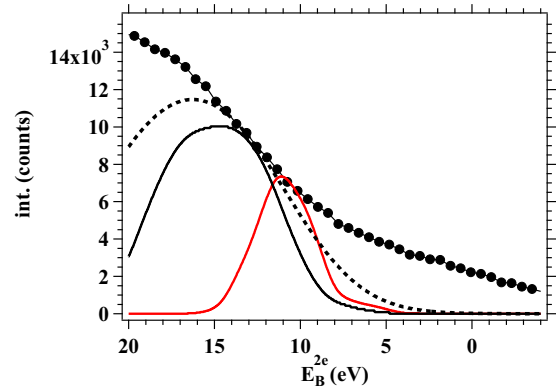

FIG. 7. We plot the $(p, 2e)$ E_{sum} spectrum from a Ag(100) surface with $E_p^+ = 42$ eV. The two-particle binding energy scale allows direct comparison with the 2e-DOS curves; see the text. The red curve is the 2e-DOS of Ag. The black curve is a superposition of the 2e-DOS curve assuming a positron energy from 0 to 8 eV. The dashed black curve is a convolution of the black curve with the experimental resolution.

$E_{\mathrm{sum}}^{\mathrm{max}}$. Most of the intensity is found below $E_{\mathrm{sum}}^{\mathrm{max}}$ mainly within a triangular shaped region near the lower left-hand corner. There is an extended region (blue colors) that is above the $E_{\mathrm{sum}}^{\mathrm{max}}$ line. This intensity is not due to "random" coincidences, because we removed the aggregate affect of the "random" intensity as explained above. In the Supplemental Material, we will discuss the origin of the intensity above $E_{\mathrm{sum}}^{\mathrm{max}}$ [22]. Key aspects are the annihilation-induced Auger emission and electron emission due to the slowing down of the positron [23–33].

For the discussion of the material dependence, we integrate over the whole 2D-energy window. This includes also the intensity above the $E_{\mathrm{sum}}^{\mathrm{max}}$ line, but this amounts to only a few percent of the total intensity and can be ignored. In Fig. 6, we show the total $(p, 2e)$ intensity as a function of the normalized singles rate. This is the electron count rate divided by the positron flux. We added to this plot our previously published data on the (p, ep) intensity [10]. Obviously the $(p, 2e)$ and (p, ep) intensities are very comparable. This is a bit of a surprise since we assumed that a sequence of two binary collisions caused the emission of an electron pair in $(p, 2e)$. In the (p, ep) process, only a single collision suffices to emit a positron-electron pair.

From Fig. 6 we see an almost monotonic relation between the singles and coincidence rate. Obviously the higher the singles rate, the higher the coincidence rate. The material with the highest rate in (p, ep) and $(p, 2e)$ is NiO. Such an observation was also made in previous $(e, 2e)$ and double photoemission experiments [6–8].

We have related this to the strength of the electron-electron interaction. NiO can be regarded as highly correlated because the description within the local density approximation (LDA) makes the erroneous prediction that this material is conducting. The experimental observation, however, is that it is an insulator. Although the electron correlation is included within the LDA, the description for NiO requires a more sophisticated approach for treating the electron correlation.

A framework for a single binary collision in $(e, 2e)$ and (p, ep) from surfaces has been formulated, and numerical results have been published [34–38]. The operator describing the transition is a screened Coulomb interaction between the two electrons that are emitted in $(e, 2e)$. In the case of (p, ep), the interaction is between the emitted positron-electron pair. Using a screened Coulomb potential is an approximation of the dielectric constant of the target material. Within this entity, the electron-electron interaction of the target material is incorporated. It is this feature that suggests that the intensity is a measure of the electron correlation strength [6].

The stronger coincidence intensity for NiO within a $(p, 2e)$ process can be conceptually understood. As indicated by Fig. 4, the first step is a (p, ep) process, and the second step is either a (p, ep) or $(e, 2e)$ scattering event. Each individual step has a higher probability to occur for NiO compared to the other materials. Therefore, we expect also that the $(p, 2e)$ intensity is highest for NiO. This also supports the view that the key contribution to the measured $(p, 2e)$ signal arises from the two-step scattering picture, as sketched in Fig. 4.

In Fig. 7, we show the E_{sum} spectrum for the $(p, 2e)$ experiment on a Ag(100) surface. The primary energy was $E_p^+ = 42$ eV. In analogy to photoemission, we use a binding-energy scale given by $E_B^{2e} = E_{\mathrm{sum}}^{\mathrm{max}} - E_{\mathrm{sum}}$. This two-particle binding energy is appropriate for comparison with the two-particle density-of-states (2e-DOS) curves given by the red and black traces, as we will explain below. It is apparent that the intensity decreases monotonically and does not display sharp features. The intensity above $E_B^{2e} = 0$ has a contribution due to primary positrons, which possess a higher kinetic energy than the peak; see Fig. 2(b). In the Supplemental Material, we discuss an additional pathway due to the annihilation of the positron, which can lead to intensity above $E_B^{2e} = 0$.

So far, the process that leads to the $(p, 2e)$ intensity (as sketched in Fig. 4) has not been theoretically discussed. Therefore, we present an approximation in which the individual steps of $(e, 2e)$ and (p, ep) are treated in the simplest picture. A consequence of the theory of $(e, 2e)$ and $(p, 2e)$ is that

the E_{sum} spectrum is largely determined by the kinematically accessible density of states (DOS) [34–38]. Of course the matrix element for a transition is not constant, but experiments have shown that the DOS can be used to identify regions in the E_{sum} spectrum from Cu(111), Cu(100), and Ag(100) surfaces [6,12,39]. With this in mind, we propose that the $(p, 2e)$ E_{sum} spectrum should be compared with the self-convolution of the density of states (2e-DOS) of the sample. This is equivalent to the description of the Auger line shape if the transition leads to two vacancies in the valence band. The 2e-DOS of Ag has been included in Fig. 7 as a red curve. We recall that the DOS of Ag can be described in simple terms as follows. The $4d$ levels with a total occupancy of 10 electrons reside in a binding-energy range from 3 to 7 eV. The strongly dispersing $5sp$ bands cover a binding-energy range from 8 eV up to E_F. Since there is only one $5sp$ electron, the DOS is dominated by the contribution of the $4d$ bands. This explains the 2e-DOS peak around 11 eV.

The 2e-DOS would be appropriate if the total kinetic energy of the positron has been transferred to the emitted valence electrons. If, on the other hand, the positron has a finite kinetic energy, the 2e-DOS would have to be shifted to the left by the positron kinetic energy. Since we are unable to record triple coincidences, we have to make assumptions about the positron kinetic energies.

Previously we have shown the positron energy spectrum from a Ag(100) surface [10]. The low-energy part displayed a peak at around 4 eV, while at 8 eV kinetic energy the intensity has half of the peak intensity. The integrated positron intensity from 0 to 8 eV amounts to about 60% of the total positron intensity. Therefore, we make the simplifying assumption that the positron energy covers a range from 0 to 8 eV with equal probability. The black curve is the average of shifted 2e-DOS curves using this positron energy width. We take into account the spectral resolution, and we obtain the black dashed curve by using a Gaussian of a FWHM of 7 eV. For presentation purposes, all curves in Fig. 7 have been scaled such that they touch the experimental data points.

Given the simplicity of our description, one cannot expect very good agreement. Yet we learn from the existence of intensity in the region $E_B^{2e} = 18$–0 eV that two binary collisions occur in which the electron pair possesses the energy lost by the positron. Compared to the simulation, we observe a higher intensity in the region above $E_B^{2e} = 10$ eV. We associate this with matrix element effects similar to those seen in $(e, 2e)$ measurements on Ag and Cu surfaces [6,12,39]. Moving toward $E_B^{2e} = 20$ eV, the experimental intensity still increases while the simulation suggests a decreasing intensity.

An obvious explanation is the excitation of more than two electrons via additional scattering events. As a matter of fact, the secondary electron due to primary particle impact is thought to occur via many electron collisions leading to a cascade. A large fraction of the secondary electrons emitted at low energies exhibits a peak at around 2 eV kinetic energy. Most of the experimental evidence is based on total yield measurements [40]. Those give no information about the energy relations among the emitted electrons.

In this sense, our measurements provide this relation. We note a close similarity in the secondary emission spectrum due to positron and electron impact, e.g., for Ag(100) [33]. Additionally, the primary energy dependence of the yield for a Ag(100) surface is almost the same for positron and electron excitation. Therefore, we can interpret our $(p, 2e)$ data as an effective $(e, 3e)$ experiment. This statement is based on the fact that positrons and electrons are distinguishable particles.

V. SUMMARY

We have discussed the $(p, 2e)$ emission from solid surfaces. Despite the fact that this has to be a two-step process, the $(p, 2e)$ intensity is of the same magnitude as those from the (p, ep) experiments. In line with our previous work on double photoemission and $(e, 2e)$, we also found for the $(p, 2e)$ pathway a relation between singles and pair emission rate. This is remarkable because of the large differences in the microscopic origin leading to pair emission. Common to all these processes is the need for a finite electron correlation, and we take our results as additional confirmation that the intensity scales with the correlation strength.

The sum energy spectrum reveals that a sizable contribution involves events in which the electron pair possesses the kinetic energy lost by the positron.

ACKNOWLEDGMENTS

The development of the positron beam benefited from suggestions by R. Krause-Rehberg and P. Coleman. We took advantage of stimulating discussions with H. Gollisch, F. Giebels, and R. Feder. We thank the Ithemba team for support and hospitality during the positron source characterization. This work was funded by the Deutsche Forschungsgemeinschaft (DFG, German Research Foundation) - Projektnumber 31047526 - SFB 762, project B7.

[1] L. Avaldi and A. Huetz, J. Phys. B **38**, S861 (2005).
[2] J. Ullrich, R. Moshammer, A. Dorn, R. Dörner, L. P. H. Schmidt, and H. Schmidt-Böcking, Rep. Prog. Phys. **66**, 1463 (2003).
[3] J. L. Powell and B. Crasemann, *Quantum Mechanics* (Dover, Mineola/New York, 2015).
[4] J. Berakdar, Phys. Rev. B **58**, 9808 (1998).
[5] B. D. Napitu and J. Berakdar, Phys. Rev. B **81**, 195108 (2010).
[6] F. O. Schumann, L. Behnke, C. H. Li, J. Kirschner, Y. Pavlyukh, and J. Berakdar, Phys. Rev. B **86**, 035131 (2012).
[7] F. O. Schumann, L. Behnke, C. H. Li, and J. Kirschner, J. Phys.: Condens. Matter **25**, 094002 (2013).
[8] F. O. Schumann, Y. Aliaev, I. Kostanovskiy, G. Di Filippo, Z. Wei, and J. Kirschner, Phys. Rev. B **93**, 235128 (2016).
[9] I. S. Brandt, Z. Wei, F. O. Schumann, and J. Kirschner, Phys. Rev. Lett. **113**, 107601 (2014).

[10] I. S. Brandt, Z. Wei, F. O. Schumann, and J. Kirschner, Phys. Rev. B **92**, 155106 (2015).
[11] G. A. van Riessen, F. O. Schumann, M. Birke, C. Winkler, and J. Kirschner, J. Phys.: Condens. Matter **20**, 442001 (2008).
[12] F. O. Schumann, R. S. Dhaka, G. A. van Riessen, Z. Wei, and J. Kirschner, Phys. Rev. B **84**, 125106 (2011).
[13] G. A. Sawatzky, Auger photoelectron coincidence spectroscopy, in *Auger Electron Spectroscopy*, edited by C. L. Briant and R. P. Messmer (Academic Press, San Diego, 1988), p. 167.
[14] E. Jensen, R. A. Bartynski, S. L. Hulbert, and E. Johnson, Rev. Sci. Instrum. **63**, 3013 (1992).
[15] S. Peacor and T. Hibma, Surf. Sci. **301**, 11 (1994).
[16] J. Wollschläger, D. Erdös, H. Goldbach, R. Höpken, and K. M. Schröder, Thin Solid Films **400**, 1 (2001).
[17] S. Grosser, C. Hagendorf, H. Neddermeyer, and W. Widdra, Surf. Interface Anal. **40**, 1741 (2008).
[18] M. Caffio, B. Cortigiani, G. Rovida, A. Atrei, C. Giovanardi, A. di Bona, and S. Valeri, Surf. Sci. **531**, 368 (2003).
[19] K. Marre and H. Neddermeyer, Surf. Sci. **287-288**, 995 (1993).
[20] K. Marre, H. Neddermeyer, A. Chassé, and P. Rennert, Surf. Sci. **357-358**, 233 (1996).
[21] P. J. Schultz and K. G. Lynn, Rev. Mod. Phys. **60**, 701 (1988).
[22] See Supplemental Material at http://link.aps.org/supplemental/10.1103/PhysRevB.100.075139 for the origin of the intensity above $E_{\mathrm{sum}}^{\mathrm{max}}$.
[23] R. Mayer and A. Weiss, Phys. Rev. B **38**, 11927 (1988).
[24] A. Weiss, R. Mayer, M. Jibaly, C. Lei, D. Mehl, and K. G. Lynn, Phys. Rev. Lett. **61**, 2245 (1988).
[25] K. O. Jensen and A. Weiss, Phys. Rev. B **41**, 3928 (1990).
[26] E. Jung, H. Q. Zhou, J. H. Kim, S. Starnes, R. Venkataraman, and A. H. Weiss, Appl. Surf. Sci. **116**, 318 (1997).
[27] J. Mayer, C. Hugenschmidt, and K. Schreckenbach, Surf. Sci. **604**, 1772 (2010).
[28] C. Hugenschmidt, J. Mayer, and K. Schreckenbach, Surf. Sci. **601**, 2459 (2007).
[29] J. Mayer, C. Hugenschmidt, and K. Schreckenbach, Phys. Rev. Lett. **105**, 207401 (2010).
[30] S. F. Mukherjee, K. Shastry, and A. H. Weiss, Phys. Rev. B **84**, 155109 (2011).
[31] R. A. Bartynski, Q. Qian, and S. L. Hulbert, J. Phys. IV (France) **09**, Pr6-157 (1999).
[32] Z. Wei, F. O. Schumann, C. H. Li, L. Behnke, G. Di Filippo, G. Stefani, and J. Kirschner, Phys. Rev. Lett. **113**, 267603 (2014).
[33] A. P. Knights and P. G. Coleman, Appl. Surf. Sci. **85**, 43 (1995).
[34] R. Feder, H. Gollisch, D. Meinert, T. Scheunemann, O. M. Artamonov, S. N. Samarin, and J. Kirschner, Phys. Rev. B **58**, 16418 (1998).
[35] U. Rücker, H. Gollisch, and R. Feder, Phys. Rev. B **72**, 214424 (2005).
[36] J. Berakdar, H. Gollisch, and R. Feder, Solid State Commun. **112**, 587 (1999).
[37] J. Berakdar, Nucl. Instrum. Methods Phys. Res., Sect. B **171**, 204 (2000).
[38] F. Giebels, H. Gollisch, and R. Feder, J. Phys.: Condens. Matter **21**, 355002 (2009).
[39] Z. Wei, F. O. Schumann, R. S. Dhaka, and J. Kirschner, Phys. Rev. B **85**, 195120 (2012).
[40] Y. Lin and D. C. Joy, Surf. Interface Anal. **37**, 895 (2005).